# Photoluminescence of Germanium-Vacancy Centers in Nanocrystalline Diamond Films: Implications for Quantum Sensing Applications



MARY JOY, Rani; POBEDINSKAS, Paulius; BOURGEOIS, Emilie; CHAKRABORTY, Tanmoy; Goerlitz, Johannes; Herrmann, Dennis; Noel, Celine; Heupel, Julia; Jannis, Daen; Gauquelin, Nicolas; D'HAEN, Jan; VERBEECK, Johan; Popov, Cyril; Houssiau, Laurent; Becher, Christoph; NESLADEK, Milos & HAENEN, Ken (2024) Photoluminescence of Germanium-Vacancy Centers in Nanocrystalline Diamond Films: Implications for Quantum Sensing Applications. In: ACS Applied Nano Materials, 7 (4) , p. 3873 -3884.

DOI: 10.1021/acsanm.3c05491
Handle: http://hdl.handle.net/1942/42561

# Photoluminescence of Germanium-Vacancy Centers in Nanocrystalline Diamond Films: Implications for Quantum Sensing Applications

*Rani Mary Joy[*], Paulius Pobedinskas, Emilie Bourgeois, Tanmoy Chakraborty[‡], Johannes Goerlitz, Dennis Herrmann, Celine Noel, Julia Heupel, Daen Jannis, Nicolas Gauquelin, Jan D'Haen, Johan Verbeeck, Cyril Popov, Laurent Houssiau, Christoph Becher, Miloš Nesládek, and Ken Haenen*

**ABSTRACT**

Point defects in diamond, promising candidates for nanoscale pressure and temperature sensing applications, are potentially scalable in polycrystalline diamond fabricated using the microwave plasma-enhanced chemical vapor deposition (MW PE CVD) technique. However, this approach introduces residual stress in the diamond films, leading to variations in the characteristic zero phonon line (ZPL) of the point defect in diamond. Here, we report the effect of residual stress on germanium-vacancy (GeV) centers in MW PE CVD nanocrystalline diamond (NCD) films fabricated using single crystal Ge as the substrate and solid dopant source. GeV ensemble formation indicated by the zero phonon line (ZPL) at ~602 nm is confirmed by room temperature (RT) photoluminescence (PL) measurements. PL mapping results show spatial non-uniformity in GeV formation along with other defects, including silicon-vacancy centers in the diamond films. The residual stress in NCD results in shifts in PL peak positions. By estimating a stress shift coefficient of (2.9 ± 0.9) nm/GPa, the GeV PL peak position in the NCD film is determined to be between 598.7 nm and 603.2 nm. A larger ground state splitting due to the strain on a GeV incorporated NCD pillar at low temperature (10 K) is

also reported. We also report the observation of intense ZPLs at RT that in some cases could be related to low Ge concentration and the surrounding crystalline environment. In addition, we also observe thicker microcrystalline diamond (MCD) films delaminate from the Ge substrate, due to film residual stress and graphitic phase at the diamond/Ge substrate interface (confirmed by electron energy loss spectroscopy). Using this approach, free-standing color center incorporated MCD film with dimensions up to 1 × 1 $cm^2$ is fabricated. Qualitative analysis using the Time-of-Flight secondary ion mass spectroscopy reveals the presence of impurities, including Ge and silicon, in the MCD film. Our experimental results will provide insights to the scalability of GeV fabrication using the MW PE CVD technique and effectively implement NCD-based nanoscale sensing applications.

Keywords: Polycrystalline diamond, chemical vapor deposition (CVD), point defects, germanium, residual stress, photoluminescence.

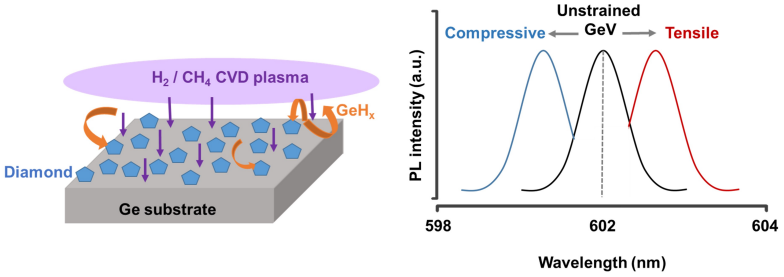

## 1. INTRODUCTION

Diamond, a potential candidate for quantum applications based on solid-state spin systems, has shown remarkable advantages in nanoscale sensing and imaging applications[1–3]. Most of these advances are based on the nitrogen-vacancy (NV) center in single crystal diamond (SCD) due to its outstanding spin coherence at room temperature (RT) and the possibility of spin readout via optically or electrically detected magnetic resonance[4,5]. However, SCD is known to be expensive and poses challenges in the scalability of the fabrication process[6,7]. In addition, the NV centers are not ideal, for example, in temperature sensing for bio-applications, as microwaves adversely influence the cell chemistry. The current temperature sensing techniques include thin-film thermocouple and fluorescent sensors based on organic dyes, quantum dots, nanoparticles[8–10]. However, these techniques have drawbacks such as heat dissipation through the substrate or limitations in sensitivity and fluorescence rate fluctuations[11].

Promising alternatives are the group IV element-vacancy color centers in diamond, where the group IV atom occupies an interstitial position between two adjacent vacancies along the <111> direction in the diamond lattice. The inversion symmetric $D_{3d}$ split-vacancy configuration results in stable emission from these color centers[12]. The group IV element-vacancy centres have advantages over the NV center - a significant amount of the fluorescence (> 70% of total emission for silicon-vacancy centers) is in the zero phonon line (ZPL) and is accompanied by a weak phonon side band[13]. In addition, the group IV color centers in diamond offer a microwave-free method for nanoscale thermometry[14–18]. Among the group IV color centers, the germanium-vacancy (GeV) center has a higher quantum efficiency than the silicon-vacancy center, thus making it an interesting candidate for temperature sensing in bio-applications[14,19].

Broadly speaking, three fabrication processes are mainly used for generating color centers in diamond[20,21]. A conventional ion implantation process has been demonstrated, enabling the creation of color centers with high spatial resolution and successfully yielding single-photon emitters[20]. However, this technique involves lattice damage and requires an annealing step at high temperatures. Other options are the high-pressure high-temperature (HPHT) and detonation nanodiamond (DND) processes, but these result in a mixture of micro- and / or nano- aggregates with impurities hence require further processing steps[15,22]. The chemical vapor deposition (CVD) technique overcomes these disadvantages by offering *in-situ* doping and large area nanocrystalline diamond (NCD) film fabrication on non-diamond substrates[23–25].

Typically, silicon is the commonly used substrate material for NCD growth studies[26]. However, the presence of silicon substrate leads to silicon vacancy (SiV) center formation in diamond[27]. One of the approaches to reduce SiV during GeV formation process is to use Ge as the substrate as well as the solid dopant source. Ralchenko *et al*. reported the direct growth of diamond on Ge substrate leading to GeV center formation in diamond[28]. However, this study does not detail the process or its challenges. Hence, the lack of knowledge on a potentially scalable fabrication process of GeV in NCD directly grown on Ge substrate using the CVD technique motivates this study.

Nanoscale sensing applications are based on the shift in ZPL position relative to the unstrained defect in diamond. However, one should note that the NCD growth on non-diamond substrates induces residual stress in diamond. The origins of residual stress are attributed to the lattice mismatch, the difference in the coefficient of thermal expansion between the diamond film and substrate and the CVD growth conditions (intrinsic stress). The stress/strain in diamond affects the ZPL position and line width of the

luminescent defect[29,30]. Therefore, for defects in NCD, it is essential to establish a correlation between residual stress and the changes in the defect ZPL. These findings can serve as a basis for implementing these defects in NCD-based applications. For example, strained GeV in NCD with residual stress can be calibrated and used for pressure sensing applications based on the ZPL shift in response to external pressure. Thus far, GeV centers in CVD diamond, fabricated using solid dopants such as germanium and its oxide or germane precursor gas, are reported[27,31–33]. However, the information on the ZPL range of strained GeV in NCD is currently lacking and forms the second motivation of our study.

Here, we report the study of residual stress-related ZPL shift of GeV in NCD film deposited on Ge substrate by microwave plasma-enhanced CVD (MW PE CVD). We systematically investigate the PL spectra and correlate peak shift to the in-plane compressive stress of the NCD film. In this way, the center wavelength range of the GeV fluorescence peak can be assigned, i.e. strained GeV centers in NCD on Ge substrate can be identified. The residual stress in the film also supports the formation of free-standing diamond films incorporated with luminescent centers. Furthermore, we report the non-uniformity of GeV formation in NCD. Consequently, we have opted for a strategy involving the transformation of the NCD film into pillars to facilitate the re-identification of GeV.

## 2. EXPERIMENTAL SECTION

Commercially available high purity single crystal 500 µm thick Ge (100) ($5 \times 5$ mm² and $1 \times 1$ cm²) were used simultaneously as substrates and the solid dopant source. The substrates were cleaned by hydrogen plasma in the ASTeX 6500 MW PE CVD system. The cleaned substrates are seeded with water-based monodispersed DND colloidal solution (NanoCarbon

Research Institute Co. Ltd, particle size 4 – 5 nm) by drop-casting followed by a deionised water rinse and spin-drying steps[34]. Diamond growth on the DND seeded substrates was carried out in the ASTeX 6500 series MW PE CVD system with process gas feed of methane and hydrogen, leading to 1% methane with a total flow of 400 sccm. The working pressure and MW power were maintained at 45 Torr and 3000 W, respectively, to ensure substrate temperature of (720 ± 20)°C, which is below the melting point of 936°C at 1 atm for Ge[35]. The substrate temperature was determined using Williamson Pro92 dual-wavelength pyrometer. The NCD growth time was 1 h and extended to 40 h for the free-standing microcrystalline diamond (MCD) film fabrication. It should be noted that once the diamond film covers the Ge substrate, it also prevents further substrate etching and thus cuts off the Ge dopant source from the plasma. Hence, additional unseeded Ge pieces were placed alongside the DND seeded substrates and in contact with the plasma form the Ge source for the 40 h deposition. For comparison, MCD film without unseeded Ge substrates was also fabricated.

Raman measurements were carried out using a 488 nm laser (Lexell SHG) with a Horiba Jobin Yvon T64000 micro-Raman spectrometer. The scanning transmission electron microscopy (STEM) combined with electron energy loss spectroscopy (EELS), used to investigate the chemical composition at the interface between Ge and diamond, was performed on the Thermo Fisher QU-Ant-EM microscope (operated at 300 kV and 20 mrad convergence angle). A focused ion beam from FEI Helios NanoLab DualBeam 650 SEM was used for cross-sectional sample preparation at the diamond/Ge interface.

The effect of stress on the photoluminescence (PL) spectra of GeV was investigated on NCD thin films which were possessing residual mechanical stress. In the case of free-standing diamond film the thermal stress, which makes the largest part of the residual stress, is eliminated after its delamination from the substrate. PL measurements of MCD film reveal GeV with ZPL of (603.3 ± 0.17) nm. The in-plane residual stress component in the NCD film

on Ge substrate was calculated using the Stoney equation[36]. The substrate curvatures before and after diamond CVD were obtained from line scan measurements with a Bruker DekTakXT® stylus profilometer. Elastic constants of the Ge substrate were taken from the literature[37].

Room temperature photoluminescence spectroscopy and mapping measurements were performed on a standard confocal setup. A 532 nm laser (Laser Quantum Gem 532) illuminated the sample. The PL response of the sample was collected onto either an avalanche photodiode (Excelitas Technologies SPCM-AQRH-14) for mapping or a charge-coupled device camera (Kymera 193i) for spectroscopy. For all measurements, the excitation with 1 mW power was focused through an objective with a numerical aperture of 0.95. A band-pass filter (ThorLabs FB600-10, CWL = (600 ± 2) nm, FWHM = (10 ± 2) nm) was used in the PL detection path for mapping mode measurements. The low-temperature PL measurements at 10 K were carried out with a liquid helium flow cryostat.

Qualitative analysis of the MCD film was carried out by the time-of-flight secondary ion mass spectroscopy (ToF-SIMS) technique. A dual-beam ToF-SIMS IV (Ion-TOF GmbH, Münster, Germany) spectrometer, allowing for an in-plane resolution of ∼1 μm, an in-depth resolution of ∼1 nm and a mass resolution $M/\Delta M$ of ∼7000 was used. In the non-interlaced bunched mode, the analysis ion beam (25 keV $Bi_3^+$, 150 × 150 μm$^2$ raster area) was operated between sputtering cycles of 10 s, using a 500 eV $Cs^+$ ion beam (400 × 400 μm$^2$ raster area). An electron flood gun was used for surface charge compensation. The profiles were acquired in negative polarity because of the higher intensity of characteristic molecular ion signals deriving from using $Cs^+$ primary ions for sputtering. Electron beam lithography and inductively coupled plasma reactive ion etching were applied to fabricate nanopillars with nominal diameters between 50 and 1000 nm. The EBL process details for structuring the NCD film to pillars can be found elsewhere[38].

## 3. RESULTS AND DISCUSSION

### 3.1 NCD Film on Ge

One of the primary process challenges of using single-crystal Ge as a dopant source and as a substrate is its melting point (936°C), which is close to the diamond deposition temperature[35]. Earlier studies report Ge substrate melting and associated surface damages, including Ge surface restructuring and pit formation partially alleviated by including thin barrier layers on Ge[39,40]**.** At first, we also observed Ge substrate melting, thus the diamond deposition temperature was limited to (720 ± 20)°C. The sources of Ge atoms could be the sublimation and the plasma etching of the Ge substrate, formation of $GeH_x$ radicals and Ge incorporation into the growing diamond layer follows, finally resulting in a GeV center in diamond[28,41,42]**.**

Figure 1 shows the SEM micrograph of the 100 nm thick NCD layer on Ge. Randomly oriented grains with well-faceted layer morphology are seen, and the characteristic peak at 1334.2 $cm^{-1}$ from Raman measurements confirm diamond formation[43]. The additional peaks in the spectrum at 1120 $cm^{-1}$ ($\nu_1$ peak), 1450 $cm^{-1}$ ($\nu_3$ peak), D- and G-bands (1350 $cm^{-1}$ and 1560 $cm^{-1}$, respectively) are related to non-diamond phases such as trans-polyacetylene and graphitic phase at the surfaces or grain boundaries of the NCD film.

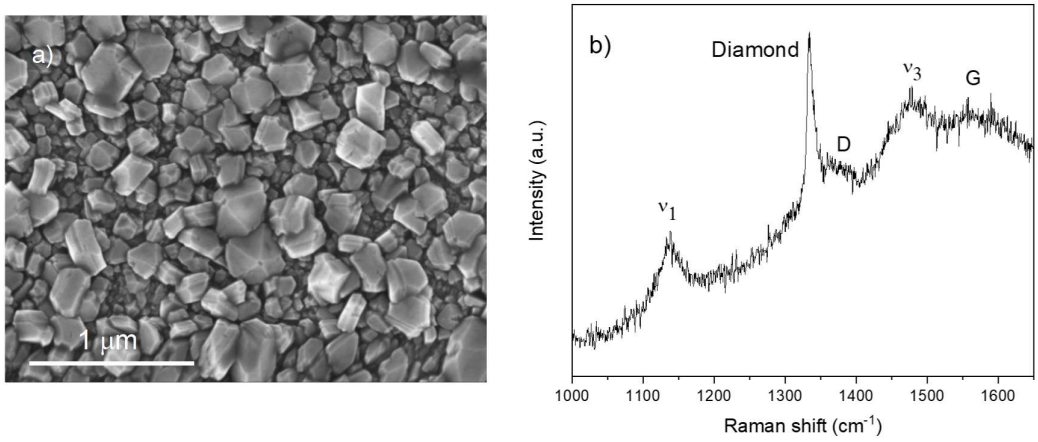


Figure 1. (a) Typical SEM image of a 100 nm thick NCD film grown on a Ge substrate and (b) a representative Raman spectrum for the NCD layer, measured at the corner position of the sample, is with the diamond peak position at 1334.2 $cm^{-1}$. Measurements carried out at multiple positions of the sample revealed comparable spectra.

Another impairing factor for diamond growth is the thermal mismatch between Ge and diamond. The linear coefficients of thermal expansion for Ge and diamond at 300 K are $5.9 \times 10^{-6}$ $K^{-1}$ and $1 \times 10^{-6}$ $K^{-1}$, respectively, and at 1000 K are $8.5 \times 10^{-6}$ $K^{-1}$ and $4.4 \times 10^{-6}$ $K^{-1}$, respectively)[39,44]. The diamond film grows on an expanded Ge substrate under CVD conditions. However, upon cooling, the substrate shrinks to its room temperature dimensions resulting in compressive stress[45]. In addition, the intrinsic stress in NCD also contributes to residual stress in the deposited diamond layer that could lead to sample bowing or even film delamination from the substrate.

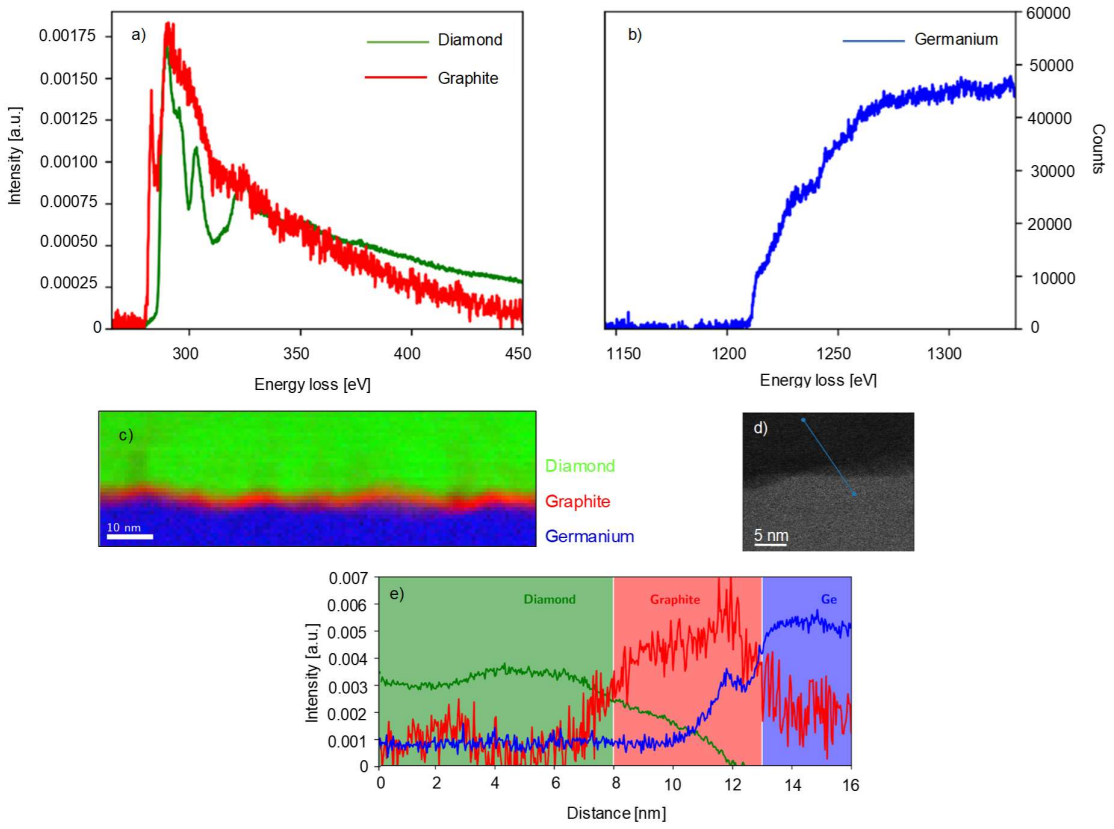


Figure 2. EELS measurement data at the NCD film /Ge substrate interface (a) diamond and graphite (b) Ge, (c) EELS mapping of diamond (green), graphite (red) and Ge (blue) (background subtracted). The colors indicate the components of the three reference spectra at every probe position. (d) The high-angle annular dark-field map with the blue line scan position over the Ge – substrate interface indicated, and (e) an overlay EELS plot for diamond graphite and Ge across the diamond interface.

Studies have shown that amorphous Ge-C form molecular fragments with low stability and Ge carbide formation is extremely small[46,47]. To investigate the chemical composition, high-resolution STEM combined with EELS was carried out at the NCD/Ge substrate interface. Figure 2 shows the EELS spectra for diamond, graphite and Ge recorded from different energy windows simultaneously. The carbon K-edge and Ge L-edge are at 284 eV and at 1217 eV,

respectively[48,49]. From the EELS mapping results, a thin graphitic layer, 2 – 5 nm thick, is seen at the diamond and Ge substrate interface. Thus, no direct chemical bonding exists between the substrate and diamond layer; observations are similar to those reported by other groups[39]. Due to the above reasons, it is challenging to grow an adherent NCD film on Ge substrate. Nevertheless, these unfavourable properties may be exploited for the fabrication of free-standing MCD films incorporated with color centers, as will be discussed in the following section.

Additionally, EELS line scan measurements were carried out at the diamond/Ge interface to determine Ge diffusion into the diamond layer. The signal from the carbon K-edge and germanium L-edge indicate that there is no diffusion of Ge into the diamond layer. The detection limit of the technique is around 0.1 at.%.

### 3.2 Ge Incorporated Free-standing Microcrystalline Diamond Film

A 9 μm thick MCD film was grown with the same plasma conditions. The growth duration of such a film was 40 h. It should be noted that once a diamond film covers the substrate, it prevents substrate-plasma interaction, thus cutting off the dopant source. Hence, additional unseeded Ge substrates were placed next to the DND seeded Ge substrate during the CVD of the MCD film. After the diamond growth, the substrate is left to cool down to room temperature in the deposition system. In addition to the differences in the thermal expansion coefficient of diamond and Ge, and the absence of the carbide interlayer, the residual stress in the diamond film drives diamond film delamination. In this way, a self-separating free-standing MCD film was fabricated (Fig. 3).

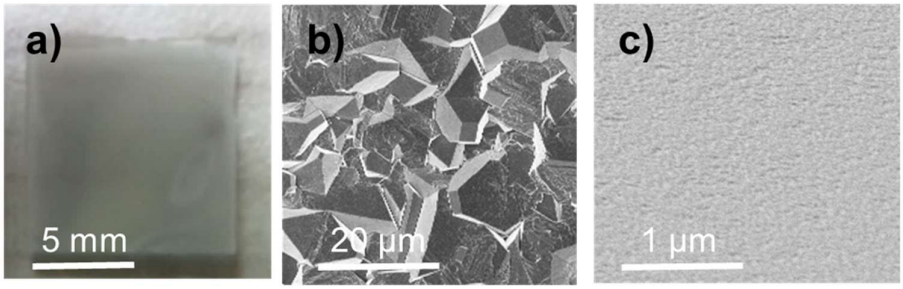


Figure 3. (a) Optical image of the free-standing microcrystalline diamond film (1 × 1 $cm^2$) and corresponding SEM images: (b) the growth and (c) nucleation sides show different film morphologies.

To find out the impurity content in the MCD film, it was analysed with ToF-SIMS. To reduce the surface roughness impact on ToF-SIMS analysis, the measurements were carried out on the nucleation side of the MCD film. Figure 4 shows a mass/charge ($m/z$) spectrum and depth profile measurement results carried out on the edges of the sample. The peak at 73.92 amu in the mass/charge spectrum confirms Ge and corresponds with Ge reference wafer measurements. Although the characterisation was carried out at random positions on the 1 × 1 $cm^2$ film, the peak was mainly observed for measurement positions close to the edges of the film. Only trace amounts of Ge could be detected at other measurement positions, which were further away from the edge.

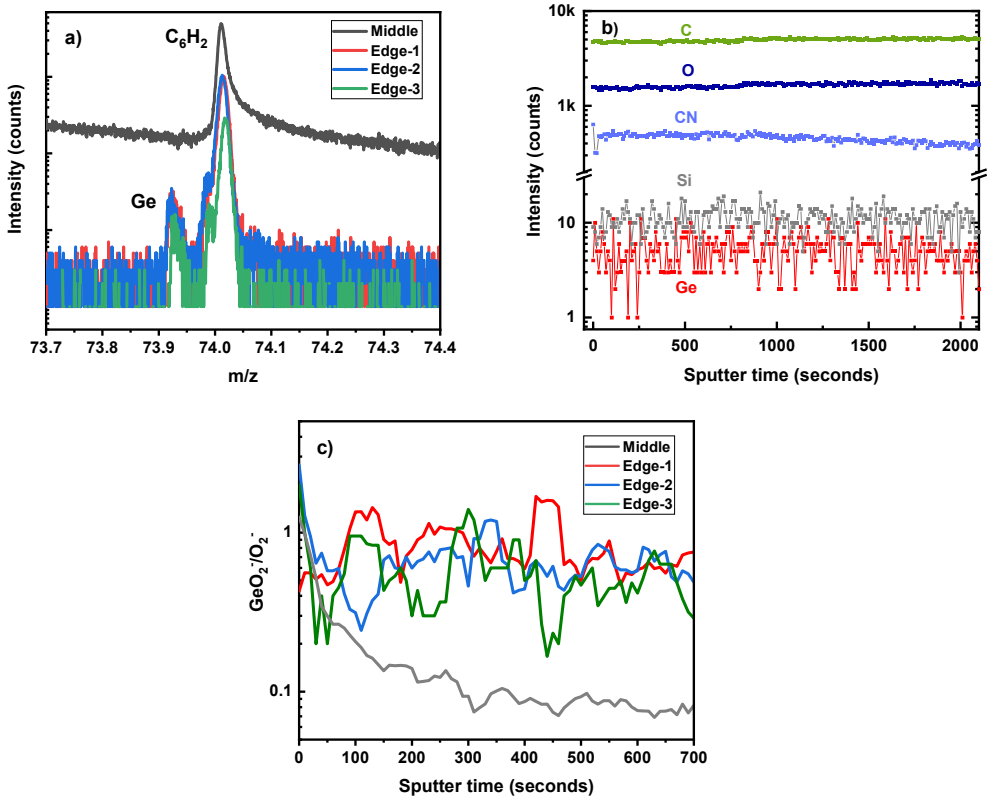


Figure 4. ToF-SIMS measurements of the free-standing microcrystalline diamond film (a) mass/charge (m/z) spectrum at different positions (edges and center) and (b) the depth profile at an edge position and (c) the ratio of $GeO_2^-/O_2^-$ at different positions.

Similar observations on preferential incorporation along the film edges have been previously reported in single crystal diamond and improved GeV formation uniformity when using additional solid dopants such as germanium oxide during diamond deposition[31]. However, the exact mechanisms for creating color centers with improved spatial uniformity are not explained. The favoured Ge incorporation along the edges may suggest a similar incorporation mechanism as additional unseeded Ge substrates were placed along the edges of the seeded Ge substrate. Grudinkin *et al.* report substrate temperature-dependent GeV formation in the hot

filament CVD process[42]. It is proposed that at temperatures near to the melting point of Ge, a quasi-liquid Ge layer forms, leading to more intense etching and, thereby, a higher concentration of $GeH_x$ radicals. Similarly, it may be the case that a temperature-related substrate edge effect, *i.e.* higher substrate temperatures are present along the Ge substrate edges, leads to higher Ge concentration at edge positions, thus, resulting in spatial non-uniformity of the Ge incorporation process. Nevertheless, the chosen diamond deposition conditions are conducive to Ge substrate etching and confirm that Ge successfully incorporates into the film during the CVD process.

The depth profiling (Fig. 4(b)) results confirm the presence of Ge, although not detected with constant signal intensity for the analysed film thickness. The ratio of $GeO_2^-/O_2^-$ analysis also confirms relatively higher Ge content at the sample edges (Fig. 4(c)). The analysis also shows additional impurities in the diamond film, the most significant being oxygen, nitrogen and silicon. High levels of oxygen and nitrogen, detected as CN, can be attributed to the low base pressure in the deposition system ($4 \times 10^{-3}$ mbar) or speculated leakage in the deposition system. Other complexes were also seen in the *m*/*z* spectrum, such as $C_6H_2$. Despite the absence of a dopant source such as silicon substrate or silane gas precursor, silicon is present in our diamond samples, with speculated sources being residual silicon or quartz parts of the CVD chamber[42]. Hence, we propose that it may be feasible to fabricate Ge-incorporated high-purity diamond films under high purity environment. Although with the ToF-SIMS technique impurities including Ge are detected, there is very little evidence if the dopant incorporation occurs in the diamond grain. The low lateral resolution of the ToF-SIMS technique restricts the analysis between crystal and grain boundaries in the diamond film.

### 3.3 Photoluminescence Measurements

The formation of GeV centers in diamond can be confirmed by PL measurements. A typical PL spectrum measured at RT is characterised by the ZPL (602.5 ± 0.5) nm with a full width at half maximum (FWHM) ranging from 4 to 5 nm for GeV ensembles in high purity single crystal diamond fabricated via CVD and via the HPHT process[28,41,50,51]. In the following sections, we discuss the RT PL spectra in our samples, followed by peak distribution and PL measurements at low temperature (10 K).

#### 3.3.1 PL of Free-standing Microcrystalline Diamond Film

Figure 5 shows a typical RT PL spectrum from the free-standing MCD film. Comparative PL studies on MCD film grown without unseeded Ge substrates were also carried out. The most prominent peak in the PL spectrum, in addition to the diamond Raman peak (572 nm), is at ~737 nm corresponding to SiV centers in diamond[52]. As mentioned in the previous section, silicon is an unintentional dopant, and its presence as SiV centers correlates well with the ToF-SIMS results. Studies on controlling SiV formation by limiting the available Si substrate surface or by co-doping techniques have been reported[27,32]. A strong and broad background fluorescence extending over the spectral measurement range are attributed to the dislocations, grain boundaries, impurities (as detected by ToF-SIMS) and the $sp^2$ phases in the polycrystalline or nanocrystalline diamond host material[53].

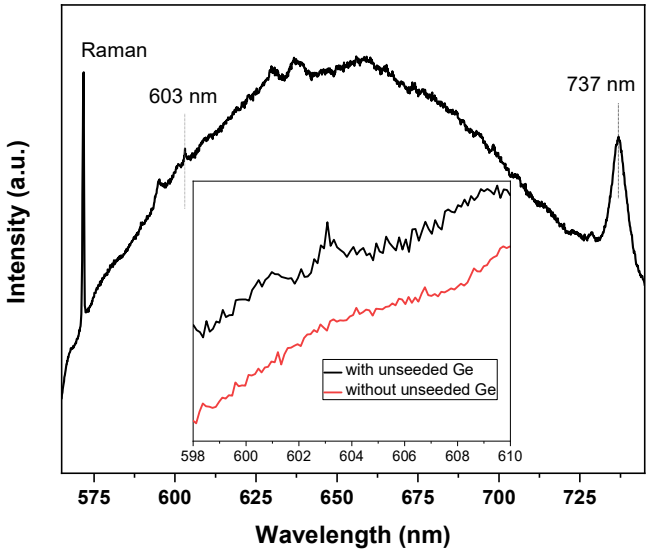


Figure 5. Typical RT PL spectrum of the free-standing microcrystalline diamond film. The inset shows the PL spectra of MCD grown with and without unseeded Ge substrates. The spectra are vertically offset for clarity.

Other less intense and identifiable peaks in the RT PL spectra are at 595 nm, 629 nm, 637 nm and 693 nm which could be identified as nitrogen-related defects, for example, negatively charged NV center (637 nm) or other nitrogen-carbon complexes[54]. These centers also have side bands and could contribute to the background of the free-standing diamond PL spectra.

### 3.3.2 PL of Nanocrystalline Diamond Film on Ge at RT

PL measurements were carried out on a 100 nm thick NCD film on Ge substrate deposited under the same depositions conditions as the MCD film. Variations in spectra measured at different sample positions are seen - some spectra have additional peaks indicating spatial non-homogeneities in the NCD film (Fig. 6).

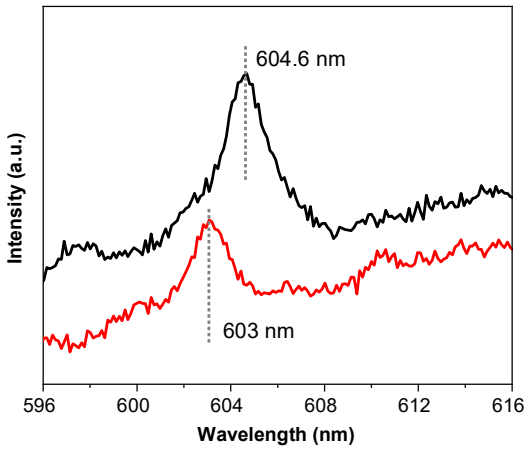


Figure 6. Examples of typical RT PL spectra of a 100 nm thick NCD film. Measurements are carried out at two random positions on the same sample.

The PL mapping (measured with a 600 nm band-pass filter) also shows areas with high intensities indicating non-uniformity in GeV formation (Fig. 7). However, one should keep in mind that NCD has a PL quenching behaviour due to the non-diamond phases and/or hydrogen surface termination[55,56]. Similar observations were reported by Eremchev *et al.* on GeV centers in CVD epitaxial diamond using germane gas as the dopant source[57]. They also observed bright and dim regions in PL, and although RT measurements did not show a GeV PL peak, some of the dim regions under cryogenic conditions revealed GeV centers in very low concentrations. Thus, the GeV ZPL may be quenched in NCD, even if the centers are created, resulting in non-uniform intensity in PL mapping.

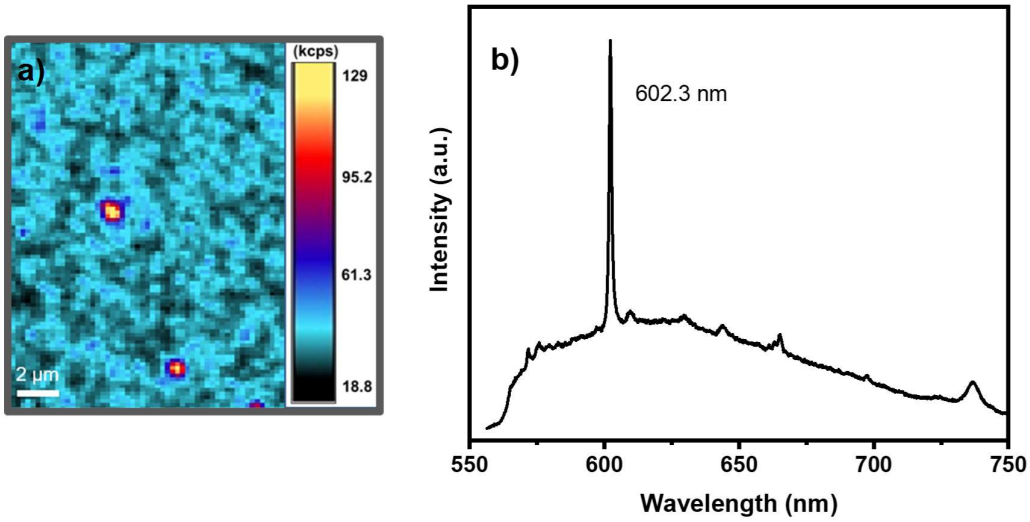


Figure 7. (a) RT PL mapping of 100 nm thick NCD film with band-pass filter and (b) an exemplary spectrum with intense ZPL measured at a bright spot in the PL mapping.

It is also interesting to note that in our samples, the GeV centers are primarily at the edge positions of the NCD film, supporting the ToF-SIMS measurements. Our experiments at slightly higher MW power resulted in substrate melting initiated at the edges. Hence, the observation suggests that GeV incorporates along the edge positions where a higher substrate temperature could be expected.

Although not frequent, we also observe intense ZPLs. The PL spectrum in Fig. 7 shows such an exemplary RT PL spectrum with an intense ZPL at 602.3 nm with FWHM of $\leq 3$ nm. Again, these spectra with intense peaks may be measured at spots where incorporation is preferred in larger crystals in the NCD layer and hence stand out from the background fluorescence. Unstrained GeV emitters have a typical RT ZPL line width of about 4 – 5 nm[50]. Narrow ZPL widths seen in SiV incorporated (001) oriented diamond nano-islands were assigned to low doping concentrations[58]. Lindner *et al.* and Görlitz *et al.* also report narrow emission lines for

SiV and tin vacancy (SnV) centers in diamond, respectively[30,59] - the deviations in ZPL position and width attributed to strain and modified electron-phonon coupling in the presence of strain. We note that a clear theoretical explanation for these experimental observations is not yet available; hence tentatively attribute the emission lines observed in our NCD samples to low doping concentrations and the surrounding crystalline environment. Whether these defects are single centers is currently unclear and will be a topic of interest in future studies.

### 3.3.3 PL Peak Shift Investigation

The position of the ZPL that corresponds to a diamond point defect changes with the isotopic constitution of the element and shifts depending on the environment of the color center; for example, the lattice strain leads to shifts in ZPL position. Detailed studies on the line positions and FWHM of SiV in nanodiamonds and diamond microstructures have been reported where peak shift and line broadening were assigned to strains in the diamond lattice[29,60]. The GeV ZPL shift from 600.5 nm to 611 nm was reported in ion-implanted samples[41], while ZPL shift of less than 0.2 nm is reported in $^{72}$Ge compared to natural Ge in HPHT diamond[50]. As can be seen in Figure 6 we also observe the variation in peak position in the PL spectra. To investigate further, measurements were carried out at multiple positions within the same sample. Figure 8 shows the peak distribution between 598 to 610 nm for the NCD film (d = 100 nm) – a red-shifted peak is more often observed than a blue-shifted peak, with the most occurrences between 602 nm and 606 nm.

The diamond Raman peak shifts towards higher or lower wavenumbers when the lattice is under compressive or tensile strain, respectively[30]. In addition, defects in the diamond lattice are the cause of the line broadening and also the shift towards higher or lower wavenumbers[60]. Figure 1(b) a representative Raman spectrum for the NCD layer, measured at the corner

position of the sample, is with the diamond peak position at 1334.2 $cm^{-1}$. Measurements carried out at multiple positions of the sample revealed comparable Raman spectra. With the shift towards higher wavenumber, the Raman measurements indicate compressive residual stress in the NCD film.

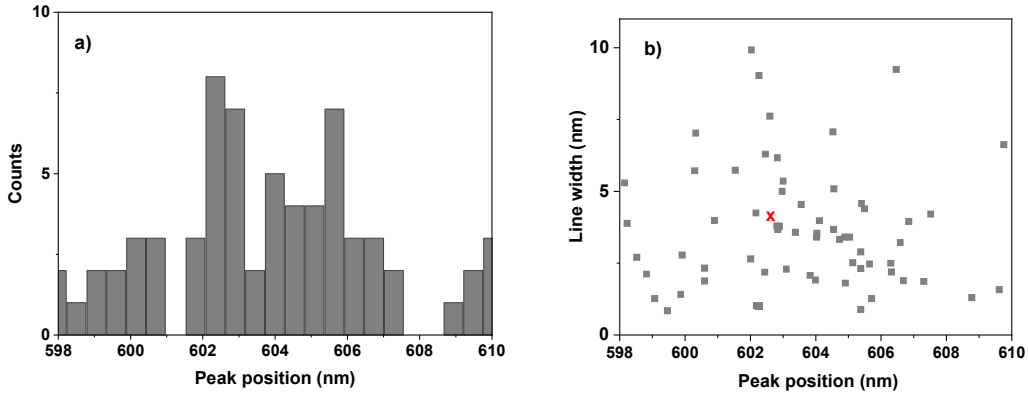


Figure 8. (a) The observed ZPL position and (b) FWHM distribution based on room temperature PL measurements on a 100 nm thick NCD film. The red cross in (b) represents unstrained GeV ensemble as reported in literature[50].

Based on the relation $\Delta\omega = \sigma \times 2.94$ [$cm^{-1}$/GPa], where $\Delta\omega$ is the Raman shift and σ is the stress[30], the residual compressive stress in the NCD film is estimated to be about (−0.6 ± 0.2) GPa. Furthermore, the in-plane residual stress was obtained by substrate curvature measurements, with and without the NCD layer, based on the Stoney equation[36]. The resulting in-plane residual stress in the NCD film was found to be compressive with a value of (−0.85 ± 0.15) GPa. The differences in stress between Raman and substrate curvature measurements are well known and explained by Prawer et al. [43].

As the NCD film residual stress is compressive, blue shifted ZPL is expected for GeV aligned in-plane with the substrate. Alternatively, the red-shifted peaks indicate out-of-plane aligned

GeV, i.e. the [111] axis of the GeV center lies in the growth direction of the NCD. It can hence be concluded from the peak distribution in Figure 8 that both in-plane and out-of-plane GeV centers are present in NCD. For biaxially strained films, the in-plane stress ($\sigma_{xx}$) and out-of-plane strain ($\varepsilon_{zz}$) are related via the Young's modulus ($E$) and Poisson ratio ($\nu$) by the relation

$$\varepsilon_{zz} = -2\,\frac{\nu}{E}\sigma_{xx} \qquad \text{(Eq. 1)}$$

If one considers for NCD a Poisson's ratio of 0.12[61], the calculated out-of-plane tensile stress is (0.21 ± 0.03) GPa. Thus, the GeV centers that undergo this tensile stress manifest as red shifted peaks in the PL spectra. With known residual stress values, the range of GeV ZPL in the peak distribution can be estimated if the stress shift coefficient (ZPL shift in nm/GPa) in NCD is also defined. Studies on voltage-deflected single-crystal diamond cantilevers demonstrate that the strain susceptibility coefficient for GeV is comparable to those of SiV centers[62,63]. Thus, by analysing the ZPL shift of SiV in NCD relative to the unstrained SiV in diamond (ZPL ~738 nm and FWHM of 4 – 5 nm) at room temperature, the stress shift coefficient can be approximated.

Figure 9 shows the ZPL position and FWHM for the SiV centers in NCD to be at (738.2 ± 0.5) nm which corresponds to a stress shift coefficient of (2.9 ± 0.9) nm/GPa. We expect a comparable value for GeV as well and hence propose the GeV ZPL in NCD to be between (598.7 ± 0.1) nm and (603.2 ± 0.1) nm. Thus, the observation of the most occurring ZPL wavelength in the GeV ZPL distribution, the peaks shifted by a few nm relative to the strain-free GeV ZPL can be explained, with the remaining peaks tentatively assigned to other fluorescent defects, such as GeV containing complexes. It should be noted that local variations in defects in NCD grains and grain boundaries also lead to variations in the local stress/strain and may also contribute additional variations in ZPL[64]. We also note that Raman peak, SiV and GeV may not be identified in the same PL spectrum. From the histograms, the GeV may be

red- or blue-shifted, while the SiV is mostly red-shifted indicating the PL peak shifts of GeV and SiV ZPLs are not necessarily correlating (Fig. S1 in supplementary data).

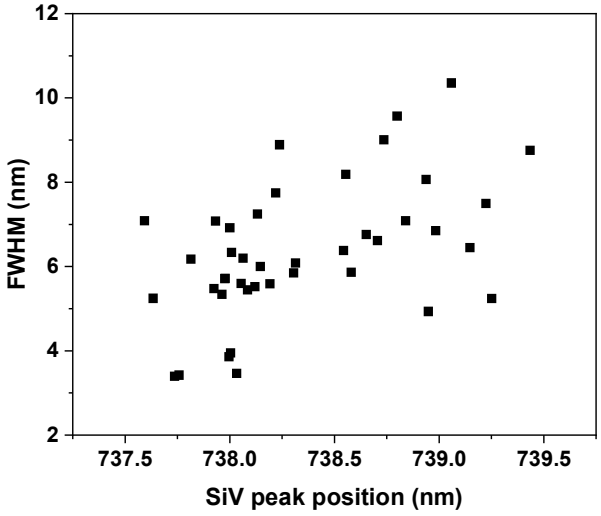


Figure 9. ZPL position and FWHM distribution for the SiV centers in 100 nm thick NCD film. The measurements are carried out at the corners of the NCD film and data obtained from same spectra used for GeV analysis.

Analysis was also carried out on the sideband peaks for the PL spectra with intense peaks (Fig. S2 in supplementary data). Theoretical and experimental studies on the local vibrational modes in neutral, ground and excited negatively charged GeV centers are reported in literature[50,65]. The localised vibrational mode for Ge is reported to be at 615 nm and another peak at 640 nm corresponding to the vibronic side band is expected for the RT PL GeV. The first and second order lines of diamond are expected at about 572 nm and 620 nm, respectively. However, these diamond features are not clearly identifiable for NCD in the PL spectra.

### 3.3.4 PL of NCD on Ge at Low Temperature (10 K)

In our samples, to facilitate the re-identification of GeV centers, the NCD film underwent a standard e-beam lithography process creating arrays of NCD pillars. Figure 10 shows representative SEM and PL mapping images of the NCD pillar under investigation. At cryogenic temperatures, the unstrained GeV PL spectrum is characterised by a four-level energy structure (Fig. 11(a)) with the ground ($\Delta E_1$) splitting by 0.75 meV (181 GHz) and excited state ($\Delta E_2$) splitting by 4.63 meV (1120 GHz)[50]. However, larger ground state splitting when the diamond lattice is under strain has also been reported[63,66].

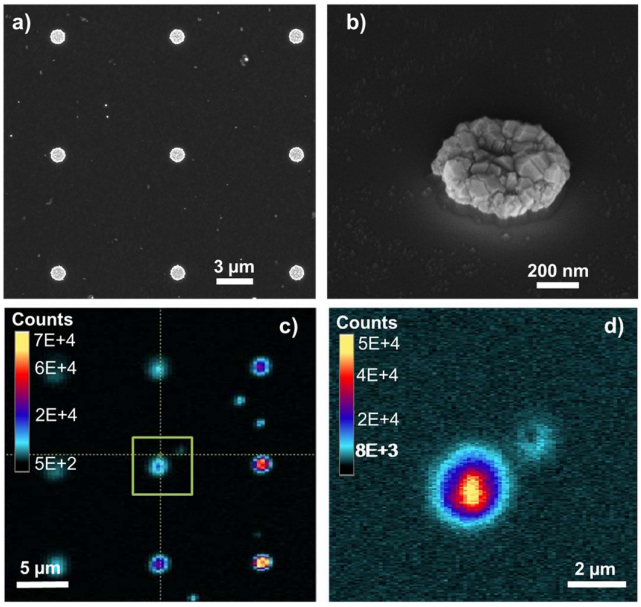


Figure 10. (a) SEM image of NCD pillar array, (b) NCD pillar at higher magnification, and the corresponding room temperature PL mapping (c,d).

An NCD pillar with RT ZPL at ~600 nm is chosen for low temperature measurements (Fig. S3 in supplementary data). Upon cooling the sample down to 10 K the GeV ZPL shifts to lower wavelengths and a complex peak structure appears (Fig. 11(b)). The observed ZPL shift in

diamond at low-temperature is known to be determined by two factors – lattice thermal contraction and the electron-phonon coupling[67]. In our case, additional thermal stress between the Ge substrate and NCD film is also present.

Studies on GeV and SnV centers in HPHT diamond show that the contribution of lattice thermal expansion is ~25% of the total ZPL shift, while the temperature-dependent line broadening and the shift were explained by the quadratic electron-phonon coupling between the electronic transition and the localised vibrational mode[68,69]. However, variations from this model have also been recently reported for low concentration GeV centers in epitaxial layers[57]. A similar observation of complex peak structures is also found in SiV and GeV ensembles under stress. Superpositioned spectra with different ZPL of GeV sub-ensembles with strain broadening is also reported in the literature[57,70].

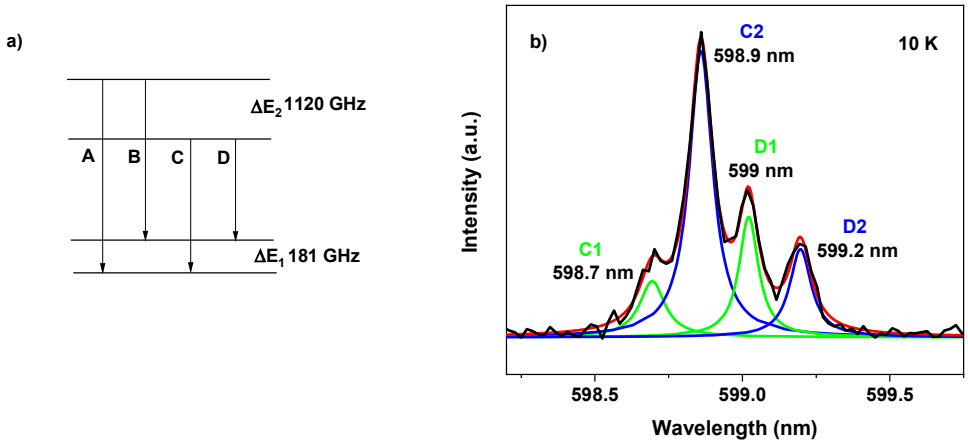


Figure 11. (a) Representation of the energy level scheme for the GeV center, (b) the low temperature (10 K) PL spectrum recorded on a GeV containing NCD pillar.

In our case, the complex structure can be deconvoluted into four peaks (Fig. 11(b)). However, the observed levels do not exactly match with the expected energies of the excited state to the splitted ground level. We have hence adapted the procedure from Grudinkin *et al.*[70], with the

best match for transition from the lower excited state to the splitted ground levels from which the ground level splitting is calculated. The ground state splitting values of 314 GHz (C1 – D1) and 266 GHz (C2 – D2) are still higher than the theoretical value of 181 GHz. We attribute this difference to the nanocrystalline character of the films and influence of strain[29,30]. Based on the work of Meesala *et al.* [62], the ground-state splitting can be estimated as a function of strain. If one considers a Young's modulus of 500 GPa for NCD, a strain value of about $4 \times 10^{-4}$ is expected for our sample, with a corresponding ground state splitting of > 800 GHz. We note that the ground state splitting in our sample is about 2.5 times lower and we attribute it to the lowering of strain on conversion of a continuous NCD film into a pillar structure. Additionally, the FWHM in the range of 0.12 – 0.16 nm may indicate the presence of single GeV centers; however, further measurements will be necessary to confirm this.

## 4. CONCLUSIONS

This work presents a comprehensive study on the *in-situ* fabrication and photoluminescence studies of GeV centers in NCD film via the MW PE CVD technique using single crystal Ge acting simultaneously as the substrate material and the solid dopant source. Despite material-associated limitations of melting point, which is close to typical diamond growth temperature, and mismatch in the coefficients of thermal expansion, we have successfully fabricated GeV centers in NCD films directly grown on the Ge substrate. Raman measurements confirmed diamond formation and SEM showed diamond film with facetted morphology.

A carbide interface is absent between the NCD/Ge substrate interface, as confirmed by the EELS measurements. The 2 to 5 nm graphitic layer at the interface corroborates no direct chemical bonding between the grown diamond film and the Ge substrate. The absence of chemical bonding and the residual stress in the film promotes the delamination of the diamond film from the Ge substrate. These make it possible to fabricate self-

delaminating free-standing color center incorporated ~9 μm thick MCD films on areas of 1 × 1 $cm^2$, as demonstrated in this study. Qualitative ToF-SIMS measurements reveal Ge with a tendency of higher detection at the diamond film edges. We suggest that such incorporation is due to higher temperature at the substrate edges.

Room temperature PL measurements confirm GeV ensemble formation with the characteristic ZPL at ~602 nm in the deposited films. We also observe the distribution of peaks between 598 to 610 nm in the NCD film, preferentially red-shifted with the most occurrences between 602 and 606 nm. Raman diamond peak analysis and substrate curvature measurements confirm compressive residual stress in the NCD film.

It can be concluded that for the blue shifted ZPL the GeV is aligned in-plane while the red-shifted peaks indicate out-of-plane aligned GeV i.e. the [111] axis of the GeV center lies in the NCD growth direction. By analysing the shift in ZPL of SiV centers, the stress shift coefficients is found to be (2.9 ± 0.9) nm/GPa. Thus, peaks between (598.7 ± 0.1) nm and (603.2 ± 0.1) nm may be explained by the in-plane and out-of plane aligned GeV centers while we tentatively assign the remaining peaks to other impurities present in the NCD layer. Analysis of the sidebands in the spectra showed various peaks probably associated with other defects.

RT PL spectrum with an intense ZPL at 602.3 nm with an FWHM of ≤ 3 nm may be indicative of low Ge doping concentration in diamond and the surrounding crystalline environment. In addition, PL measurements at 10 K on NCD pillars reveal complex ZPL structure that is speculated to originate from single GeV centers but experiencing different strained conditions. Whether the interactions with grain boundaries are significant remains an open question. Our experimental results offer insights into facilitating the implementation of strained GeV centres in NCD for nanoscale sensing applications and the scalability of GeV fabrication using the MW PE CVD technique.

## ASSOCIATED CONTENT

Supporting Information

Examples of room temperature PL spectra and a plot showing the correlation between PL peaks and silicon vacancy ZPL.

## AUTHOR INFORMATION

Corresponding Author

Rani Mary Joy – Institute for Materials Research (IMO), Hasselt University, Wetenschapspark 1, 3590 Diepenbeek, Belgium; IMOMEC, Interuniversity MicroElectronics Center (IMEC) vzw, Wetenschapspark 1, 3590 Diepenbeek, Belgium; orcid.org/0000-0001-8741-4908; Email: rani.maryjoy@uhasselt.be

**Authors**

Paulius Pobedinskas – Institute for Materials Research (IMO), Hasselt University, Wetenschapspark 1, 3590 Diepenbeek, Belgium; IMOMEC, Interuniversity MicroElectronics Center (IMEC) vzw, Wetenschapspark 1, 3590 Diepenbeek, Belgium; orcid.org/0000-0001-8136-5172

Emilie Bourgeois – Institute for Materials Research (IMO), Hasselt University, Wetenschapspark 1, 3590 Diepenbeek, Belgium; IMOMEC, Interuniversity MicroElectronics Center (IMEC) vzw, Wetenschapspark 1, 3590 Diepenbeek, Belgium; orcid.org/0000-0002-3668-1202

Tanmoy Chakraborty – Institute for Materials Research (IMO), Hasselt University, Wetenschapspark 1, 3590 Diepenbeek, Belgium; IMOMEC, Interuniversity MicroElectronics Center (IMEC) vzw, Wetenschapspark 1, 3590 Diepenbeek, Belgium; ‡Present address:

QuTech / Kavli Institute of Nanoscience, Delft University of Technology, Lorentzweg 1, 2628 CJ Delft, The Netherlands

Johannes Goerlitz – Fachrichtung Physik, Universität des Saarlandes, Campus E2.6, D-66123, Saarbrücken, Germany; orcid.org/0000-0001-5790-6354

Dennis Herrmann – Fachrichtung Physik, Universität des Saarlandes, Campus E2.6, D-66123, Saarbrücken, Germany; orcid.org/0000-0003-2761-1699

Céline Noël – Interuniversity MicroElectronics Center (IMEC) vzw, Kapeldreef 75, 3001, Leuven, Belgium

Julia Heupel – Instituts für Nanostrukturtechnologie und Analytik (INA) / Center for Interdisciplinary Nanostructure Science and Technology (CINSaT) University of Kassel, Heinrich-Plett-Str. 40, 34132 Kassel, Germany

Daen Jannis – Electron Microscopy for Materials Research (EMAT), University of Antwerp, Campus Groenenborger, Groenenborgerlaan 171, 2020 Belgium; NANOLab, University of Antwerp, Campus Groenenborger, Groenenborgerlaan 171, 2020 Belgium; orcid.org/0000-0003-0285-0511

Nicolas Gauquelin – Electron Microscopy for Materials Research (EMAT), University of Antwerp, Campus Groenenborger, Groenenborgerlaan 171, 2020 Belgium; NANOLab, University of Antwerp, Campus Groenenborger, Groenenborgerlaan 171, 2020 Belgium; orcid.org/0000-0002-5555-7055

Jan D'Haen – Institute for Materials Research (IMO), Hasselt University, Wetenschapspark 1, 3590 Diepenbeek, Belgium; IMOMEC, Interuniversity MicroElectronics Center (IMEC) vzw, Wetenschapspark 1, 3590 Diepenbeek, Belgium; orcid.org/0000-0003-4487-3885

Johan Verbeeck – Electron Microscopy for Materials Research (EMAT), University of Antwerp, Campus Groenenborger, Groenenborgerlaan 171, 2020 Belgium; NANOLab,

University of Antwerp, Campus Groenenborger, Groenenborgerlaan 171, 2020 Belgium; orcid.org/0000-0002-7151-8101

Cyril Popov – Instituts für Nanostrukturtechnologie und Analytik (INA) / Center for Interdisciplinary Nanostructure Science and Technology (CINSaT) University of Kassel, Heinrich-Plett-Str. 40, 34132 Kassel, Germany

Laurent Houssiau – Namur Institute of Structured Matter (NISM), University of Namur, Rue de Bruxelles 61, 5000, Namur, Belgium; orcid.org/0000-0003-4923-5698

Christoph Becher – Fachrichtung Physik, Universität des Saarlandes, Campus E2.6, D-66123, Saarbrücken, Germany; orcid.org/0000-0003-4645-6882

Miloš Nesládek – Institute for Materials Research (IMO), Hasselt University, Wetenschapspark 1, 3590, Diepenbeek, Belgium; IMOMEC, IMEC vzw, Wetenschapspark 1, 3590, Diepenbeek, Belgium; orcid.org/0000-0003-0215-5033

Ken Haenen – Institute for Materials Research (IMO), Hasselt University, Wetenschapspark 1, 3590, Diepenbeek, Belgium; IMOMEC, IMEC vzw, Wetenschapspark 1, 3590, Diepenbeek, Belgium; orcid.org/0000-0001-6711-7367

## ACKNOWLEDGEMENTS

This work was financially supported by the the Special Research Fund (BOF) via the Methusalem NANO network, interuniversity BOF (BOF 23IU12) and the Research Foundation – Flanders Strategic Basic Research project “DIAQUANT” (S004018N). The authors also acknowledge the support from FWO (Funds for Scientific Research Flanders), projects No. G0D1721N and No. G0A0520N Grand Challenge i-BOF UHasselt project: 'Nanoscale diamond probes to modulate temperature-sensitive ion channels in neurons and phagocyte'. JV, NG and DJ acknowledge funding from FWO project G042920N 'Coincident event detection for advanced spectroscopy in transmission electron

microscopy'. The authors also thank Dr. Nina Felgen (University of Kassel) for the technical assistance and fruitful discussions, as well as Essraa Ahmed and Giridharan Krishnamurthy (Hasselt University) for checking the validity of Raman spectra. J.H., C.P., D.H., J.G. and C.B. gratefully acknowledge funding from the German Federal Ministry of Education and Research (Bundesministerium für Bildung und Forschung, BMBF) within the project Quantenrepeater.Link QR.X (Contracts No. 16KISQ001K and 16KISQ005).

**Author Contributions**

Rani Mary Joy: Conceptualization, Methodology, Validation, Investigation, Data curation, Formal analysis, Writing – original draft, Writing – review & editing, Visualization. Paulius Pobedinskas: Conceptualization, Investigation, Data curation, Validation, Writing – review & editing, Supervision. Emilie Bourgeois: Investigation, Data curation, Validation. Tanmoy Chakraborty, Johannes Goerlitz, Dennis Herrmann, Celine Noël, Julia Heupel, Daen Jannis, Nicolas Gauquelin: Investigation, Data curation. Jan D'Haen: Investigation, Data curation, Resources. Johan Verbeeck, Cyril Popov: Supervision, Resources, Funding acquisition. Laurent Houssiau: Data curation, Formal analysis, Resources. Christoph Becher, Milos Nesládek: Supervision, Resources. Ken Haenen: Conceptualization, Writing – review & editing, Supervision, Project administration, Funding acquisition.

**Conflicts of interest**

There are no conflicts to declare.

**REFERENCES**

(1) Wrachtrup, J.; Jelezko, F. Processing Quantum Information in Diamond. *J. Phys.*

*Condens. Matter* **2006**, *18* (21), 807–824. https://doi.org/10.1088/0953-8984/18/21/S08.

(2) Aharonovich, I.; Greentree, A. D.; Prawer, S. Diamond Photonics. *Nat. Photonics* **2011**, *5* (7), 397–405. https://doi.org/10.1038/nphoton.2011.54.

(3) Schirhagl, R.; Chang, K.; Loretz, M.; Degen, C. L. Nitrogen-Vacancy Centers in Diamond: Nanoscale Sensors for Physics and Biology. *Annu. Rev. Phys. Chem.* **2014**, *65* (1), 83–105. https://doi.org/10.1146/annurev-physchem-040513-103659.

(4) Chipaux, M.; Tallaire, A.; Achard, J.; Pezzagna, S.; Meijer, J.; Jacques, V.; Roch, J. F.; Debuisschert, T. Magnetic Imaging with an Ensemble of Nitrogen Vacancy-Centers in Diamond. *Eur. Phys. J. D* **2015**, *69* (7), 1–10. https://doi.org/10.1140/epjd/e2015-60080-1.

(5) Bourgeois, E.; Gulka, M.; Nesladek, M. Photoelectric Detection and Quantum Readout of Nitrogen-Vacancy Center Spin States in Diamond. *Adv. Opt. Mater.* **2020**, *8* (12), 1902132. https://doi.org/10.1002/adom.201902132.

(6) Schreck, M.; Gsell, S.; Brescia, R.; Fischer, M. Ion Bombardment Induced Buried Lateral Growth: The Key Mechanism for the Synthesis of Single Crystal Diamond Wafers. *Sci. Rep.* **2017**, *7* (1), 44462. https://doi.org/10.1038/srep44462.

(7) Yamada, H.; Chayahara, A.; Mokuno, Y.; Kato, Y.; Shikata, S. A 2-in. Mosaic Wafer Made of a Single-Crystal Diamond. *Appl. Phys. Lett.* **2014**, *104* (10), 102110. https://doi.org/10.1063/1.4868720.

(8) Yang, N.; Xu, J.; Wang, F.; Yang, F.; Han, D.; Xu, S. Thermal Probing Techniques for a Single Live Cell. *Sensors* **2022**, *22* (14). https://doi.org/10.3390/s22145093.

(9) Okabe, K.; Sakaguchi, R.; Shi, B.; Kiyonaka, S. Intracellular Thermometry with Fluorescent Sensors for Thermal Biology. *Pflugers Arch. Eur. J. Physiol.* **2018**, *470* (5), 717–731. https://doi.org/10.1007/s00424-018-2113-4.

(10) Bradac, C.; Lim, S. F.; Chang, H. C.; Aharonovich, I. Optical Nanoscale Thermometry: From Fundamental Mechanisms to Emerging Practical Applications. *Adv. Opt. Mater.* **2020**, *8* (15), 1–29. https://doi.org/10.1002/adom.202000183.

(11) Kucsko, G.; Maurer, P. C.; Yao, N. Y.; Kubo, M.; Noh, H. J.; Lo, P. K.; Park, H.; Lukin, M. D. Nanometre-Scale Thermometry in a Living Cell. *Nature* **2013**, *500* (7460), 54–58. https://doi.org/10.1038/nature12373.

(12) Iwasaki, T. Color Centers Based on Heavy Group-IV Elements. In *Semiconductors and Semimetals*; Elsevier, 2020; Vol. 103, pp 237–256. https://doi.org/10.1016/bs.semsem.2020.03.007.

(13) Bradac, C.; Gao, W.; Forneris, J.; Trusheim, M. E.; Aharonovich, I. Quantum Nanophotonics with Group IV Defects in Diamond. *Nat. Commun.* **2019**, *10* (1), 1–13. https://doi.org/10.1038/s41467-019-13332-w.

(14) Fan, J. W.; Cojocaru, I.; Becker, J.; Fedotov, I. V.; Alkahtani, M. H. A.; Alajlan, A.; Blakley, S.; Rezaee, M.; Lyamkina, A.; Palyanov, Y. N.; Borzdov, Y. M.; Yang, Y. P.; Zheltikov, A.; Hemmer, P.; Akimov, A. V. Germanium-Vacancy Color Center in Diamond as a Temperature Sensor. *ACS Photonics* **2018**, *5* (3), 765–770. https://doi.org/10.1021/acsphotonics.7b01465.

(15) Fujiwara, M.; Fu, H.; Hariki, N.; Ohki, I.; Makino, Y.; Liu, M.; Tsurui, A.; Yoshikawa, T.; Nishikawa, M.; Mizuochi, N. Germanium-Vacancy Centers in Detonation Nanodiamond for All-Optical Nanoscale Thermometry. *Appl. Phys. Lett.* **2023**, *123* (18). https://doi.org/10.1063/5.0168194.

(16) Blakley, S.; Liu, X.; Fedotov, I.; Cojocaru, I.; Vincent, C.; Alkahtani, M.; Becker, J.; Kieschnick, M.; Lühman, T.; Meijer, J.; Hemmer, P.; Akimov, A.; Scully, M.; Zheltikov, A. Fiber-Optic Quantum Thermometry with Germanium-Vacancy Centers in Diamond. *ACS Photonics* **2019**, *6* (7), 1690–1693.

https://doi.org/10.1021/acsphotonics.9b00206.

(17) Alkahtani, M.; Cojocaru, I.; Liu, X.; Herzig, T.; Meijer, J.; Küpper, J.; Lühmann, T.; Akimov, A. V.; Hemmer, P. R. Tin-Vacancy in Diamonds for Luminescent Thermometry. *Appl. Phys. Lett.* **2018**, *112* (24), 241902. https://doi.org/10.1063/1.5037053.

(18) Fedotov, I. V.; Solotenkov, M. A.; Pochechuev, M. S.; Ivashkina, O. I.; Kilin, S. Y.; Anokhin, K. V.; Zheltikov, A. M. All-Optical Brain Thermometry in Freely Moving Animals. *ACS Photonics* **2020**, *7* (12), 3353–3360. https://doi.org/10.1021/acsphotonics.0c00706.

(19) Bhaskar, M. K.; Sukachev, D. D.; Sipahigil, A.; Evans, R. E.; Burek, M. J.; Nguyen, C. T.; Rogers, L. J.; Siyushev, P.; Metsch, M. H.; Park, H.; Jelezko, F.; Lončar, M.; Lukin, M. D. Quantum Nonlinear Optics with a Germanium-Vacancy Color Center in a Nanoscale Diamond Waveguide. *Phys. Rev. Lett.* **2017**, *118* (22), 1–4. https://doi.org/10.1103/PhysRevLett.118.223603.

(20) Pezzagna, S.; Rogalla, D.; Wildanger, D.; Meijer, J.; Zaitsev, A. Creation and Nature of Optical Centres in Diamond for Single-Photon Emission-Overview and Critical Remarks. *New J. Phys.* **2011**, *13*, 035024. https://doi.org/10.1088/1367-2630/13/3/035024.

(21) Smith, J. M.; Meynell, S. A.; Bleszynski Jayich, A. C.; Meijer, J. Colour Centre Generation in Diamond for Quantum Technologies. *Nanophotonics* **2019**, *8* (11), 1889–1906. https://doi.org/10.1515/nanoph-2019-0196.

(22) Ekimov, E. A.; Kondrin, M. V. Vacancy-Impurity Centers in Diamond: Perspectives of Synthesis and Applications. *Uspekhi Fiz. Nauk* **2017**, *187* (06), 577–598. https://doi.org/10.3367/UFNr.2016.11.037959.

(23) Bolshakov, A.; Ralchenko, V.; Sedov, V.; Khomich, A.; Vlasov, I.; Khomich, A.;

Trofimov, N.; Krivobok, V.; Nikolaev, S.; Khmelnitskii, R.; Saraykin, V. Photoluminescence of SiV Centers in Single Crystal CVD Diamond in Situ Doped with Si from Silane. *Phys. Status Solidi Appl. Mater. Sci.* **2015**, *212* (11), 2525–2532. https://doi.org/10.1002/pssa.201532174.

(24) Kromka, A.; Babchenko, O.; Izak, T.; Hruska, K.; Rezek, B. Linear Antenna Microwave Plasma CVD Deposition of Diamond Films over Large Areas. *Vacuum* **2012**, *86* (6), 776–779. https://doi.org/10.1016/j.vacuum.2011.07.008.

(25) Nicley, S. S.; Drijkoningen, S.; Pobedinskas, P.; Raymakers, J.; Maes, W.; Haenen, K. Growth of Boron-Doped Diamond Films on Gold-Coated Substrates with and without Gold Nanoparticle Formation. *Cryst. Growth Des.* **2019**, *19* (6), 3567–3575. https://doi.org/10.1021/acs.cgd.9b00488.

(26) Williams, O. A. Nanocrystalline Diamond. *Diam. Relat. Mater.* **2011**, *20* (5–6), 621–640. https://doi.org/10.1016/j.diamond.2011.02.015.

(27) Malykhin, S.; Mindarava, Y.; Ismagilov, R.; Jelezko, F.; Obraztsov, A. Control of NV, SiV and GeV Centers Formation in Single Crystal Diamond Needles. *Diam. Relat. Mater.* **2022**, *125* (March), 109007. https://doi.org/10.1016/j.diamond.2022.109007.

(28) Ralchenko, V. G. G.; Sedov, V. S. S.; Khomich, A. A. A.; Krivobok, V. S. S.; Nikolaev, S. N. N.; Savine, S. S.; Vlasov, I. I. I.; Konov, V. I. I.; Savin, S. S.; Vlasov, I. I. I.; Konov, V. I. I. Observation of the Ge-Vacancy Color Center in Microcrystalline Diamond Films. *Bull. Lebedev Phys. Inst.* **2015**, *42* (6), 157–164. https://doi.org/10.3103/S1068335615060019.

(29) Rogers, L. J.; Wang, O.; Liu, Y.; Antoniuk, L.; Osterkamp, C.; Davydov, V. A.; Agafonov, V. N.; Filipovski, A. B.; Jelezko, F.; Kubanek, A. Single Si-V-Centers in Low-Strain Nanodiamonds with Bulklike Spectral Properties and Nanomanipulation Capabilities. *Phys. Rev. Appl.* **2019**, *11* (2), 024073.

https://doi.org/10.1103/PhysRevApplied.11.024073.

(30) Lindner, S.; Bommer, A.; Muzha, A.; Krueger, A.; Gines, L.; Mandal, S.; Williams, O.; Londero, E.; Gali, A.; Becher, C. Strongly Inhomogeneous Distribution of Spectral Properties of Silicon-Vacancy Color Centers in Nanodiamonds. *New J. Phys.* **2018**, *20* (11), 115002. https://doi.org/10.1088/1367-2630/aae93f.

(31) Trycz, A.; Regan, B.; Kianinia, M.; Bray, K.; Toth, M.; Aharonovich, I. Bottom up Engineering of Single Crystal Diamond Membranes with Germanium Vacancy Color Centers. *Opt. Mater. Express* **2019**, *9* (12), 4708. https://doi.org/10.1364/OME.9.004708.

(32) De Feudis, M.; Tallaire, A.; Nicolas, L.; Brinza, O.; Goldner, P.; Hétet, G.; Bénédic, F.; Achard, J. Large-Scale Fabrication of Highly Emissive Nanodiamonds by Chemical Vapor Deposition with Controlled Doping by SiV and GeV Centers from a Solid Source. *Adv. Mater. Interfaces* **2020**, *7* (2), 1–7. https://doi.org/10.1002/admi.201901408.

(33) Sedov, V.; Martyanov, A.; Savin, S.; Bolshakov, A.; Bushuev, E.; Khomich, A.; Kudryavtsev, O.; Krivobok, V.; Nikolaev, S.; Ralchenko, V. Growth of Polycrystalline and Single-Crystal CVD Diamonds with Bright Photoluminescence of Ge-V Color Centers Using Germane GeH4 as the Dopant Source. *Diam. Relat. Mater.* **2018**, *90* (October), 47–53. https://doi.org/10.1016/j.diamond.2018.10.001.

(34) Pobedinskas, P.; Degutis, G.; Dexters, W.; D'Haen, J.; Van Bael, M. K.; Haenen, K. Nanodiamond Seeding on Plasma-Treated Tantalum Thin Films and the Role of Surface Contamination. *Appl. Surf. Sci.* **2021**, *538*, 148016. https://doi.org/10.1016/j.apsusc.2020.148016.

(35) Hall, H. T. The Melting Point of Germanium as a Function of Pressure to 180,000 Atmospheres. *J. Phys. Chem.* **1955**, *59* (11), 1144–1146.

https://doi.org/10.1021/j150533a006.

(36) Janssen, G. C. A. M.; Abdalla, M. M.; van Keulen, F.; Pujada, B. R.; van Venrooy, B. Celebrating the 100th Anniversary of the Stoney Equation for Film Stress: Developments from Polycrystalline Steel Strips to Single Crystal Silicon Wafers. *Thin Solid Films* **2009**, *517* (6), 1858–1867. https://doi.org/10.1016/j.tsf.2008.07.014.

(37) Wortman, J. J.; Evans, R. A. Young's Modulus, Shear Modulus, and Poisson's Ratio in Silicon and Germanium. *J. Appl. Phys.* **1965**, *36* (1), 153–156. https://doi.org/10.1063/1.1713863.

(38) Schmidt, A.; Naydenov, B.; Jelezko, F.; Reithmaier, J. P.; Popov, C. Fabrication of Highly Dense Arrays of Nanocrystalline Diamond Nanopillars with Integrated Silicon-Vacancy Color Centers during the Growth. *Opt. Mater. Express* **2019**, *9* (12), 4545. https://doi.org/10.1364/ome.9.004545.

(39) Rego, C. A.; May, P. W.; Williamson, E. C.; Ashfold, M. N. R.; Chia, Q. S.; Rosser, K. N.; Everitt, N. M. CVD Diamond Growth on Germanium for IR Window Applications. *Diam. Relat. Mater.* **1994**, *3* (4–6), 939–941. https://doi.org/10.1016/0925-9635(94)90304-2.

(40) Babchenko, O.; Kozak, H.; Izak, T.; Stuchlik, J.; Remes, Z.; Rezek, B.; Kromka, A. Fabrication of Diamond-Coated Germanium ATR Prisms for IR-Spectroscopy. *Vib. Spectrosc.* **2016**, *84*, 67–73. https://doi.org/10.1016/j.vibspec.2016.03.002.

(41) Iwasaki, T.; Ishibashi, F.; Miyamoto, Y.; Doi, Y.; Kobayashi, S.; Miyazaki, T.; Tahara, K.; Jahnke, K. D.; Rogers, L. J.; Naydenov, B.; Jelezko, F.; Yamasaki, S.; Nagamachi, S.; Inubushi, T.; Mizuochi, N.; Hatano, M. Germanium-Vacancy Single Color Centers in Diamond. *Sci. Rep.* **2015**, *5*, 1–7. https://doi.org/10.1038/srep12882.

(42) Grudinkin, S. A.; Feoktistov, N. A.; Bogdanov, K. V.; Baranov, A. V.; Golubev, V. G. Photoluminescence of Germanium-Vacancy Color Centers in Diamond Particles

Obtained by Chemical Vapor Deposition. *Phys. Solid State* **2020**, *62* (5), 919–925. https://doi.org/10.1134/S106378342005008X.

(43) Prawer, S.; Nemanich, R. J. Raman Spectroscopy of Diamond and Doped Diamond. *Philos. Trans. R. Soc. London. Ser. A Math. Phys. Eng. Sci.* **2004**, *362* (1824), 2537–2565. https://doi.org/10.1098/rsta.2004.1451.

(44) May, P. W. Diamond Thin Films: A 21st-Century Material. *Trans. R. Soc. Lond. A* **2000**, *358*, 473–495.

(45) Drijkoningen, S.; Janssens, S. D.; Pobedinskas, P.; Koizumi, S.; Van Bael, M. K.; Haenen, K. The Pressure Sensitivity of Wrinkled B-Doped Nanocrystalline Diamond Membranes. *Sci. Rep.* **2016**, *6* (1), 35667. https://doi.org/10.1038/srep35667.

(46) White, S. B.; McKenzie, D. R. An Electron Diffraction Study of Amorphous Hydrogenated Germanium-Carbon Thin Films. *J. Appl. Phys.* **1990**, *68* (7), 3194–3197. https://doi.org/10.1063/1.346369.

(47) Weber, W. H.; Yang, B. K.; Krishnamurthy, M. The Ge-C Local Mode in Epitaxial GeC and Ge-Rich GeSiC Alloys. *Appl. Phys. Lett.* **1998**, *73* (5), 626–628. https://doi.org/10.1063/1.121877.

(48) Hamon, A. L.; Verbeeck, J.; Schryvers, D.; Benedikt, J.; Sanden, R. M. C. M. V. D. ELNES Study of Carbon K-Edge Spectra of Plasma Deposited Carbon Films. *J. Mater. Chem.* **2004**, *14* (13), 2030–2035. https://doi.org/10.1039/b406468m.

(49) Jany, B. R.; Gauquelin, N.; Willhammar, T.; Nikiel, M.; Van Den Bos, K. H. W.; Janas, A.; Szajna, K.; Verbeeck, J.; Van Aert, S.; Van Tendeloo, G.; Krok, F. Controlled Growth of Hexagonal Gold Nanostructures during Thermally Induced Self-Assembling on Ge(001) Surface. *Sci. Rep.* **2017**, *7*. https://doi.org/10.1038/srep42420.

(50) Ekimov, E. A.; Lyapin, S. G.; Boldyrev, K. N.; Kondrin, M. V.; Khmelnitskiy, R.; Gavva, V. A.; Kotereva, T. V.; Popova, M. N. Germanium–Vacancy Color Center in

Isotopically Enriched Diamonds Synthesized at High Pressures. *JETP Lett.* **2015**, *102* (11), 701–706. https://doi.org/10.1134/S0021364015230034.

(51) Palyanov, Y. N.; Kupriyanov, I. N.; Borzdov, Y. M.; Khokhryakov, A. F.; Surovtsev, N. V. High-Pressure Synthesis and Characterization of Ge-Doped Single Crystal Diamond. *Cryst. Growth Des.* **2016**, *16* (6), 3510–3518. https://doi.org/10.1021/acs.cgd.6b00481.

(52) Neu, E.; Steinmetz, D.; Riedrich-Möller, J.; Gsell, S.; Fischer, M.; Schreck, M.; Becher, C. Single Photon Emission from Silicon-Vacancy Colour Centres in Chemical Vapour Deposition Nano-Diamonds on Iridium. *New J. Phys.* **2011**, *13* (2), 025012. https://doi.org/10.1088/1367-2630/13/2/025012.

(53) Bergman, L.; McClure, M. T.; Glass, J. T.; Nemanich, R. J. The Origin of the Broadband Luminescence and the Effect of Nitrogen Doping on the Optical Properties of Diamond Films. *J. Appl. Phys.* **1994**, *76* (5), 3020–3027. https://doi.org/10.1063/1.357508.

(54) Zaitsev, A. M. *Optical Properties of Diamond*; Springer Berlin Heidelberg: Berlin, Heidelberg, 2001; Vol. 1. https://doi.org/10.1007/978-3-662-04548-0.

(55) Yang, B.; Yu, B.; Li, H.; Huang, N.; Liu, L.; Jiang, X. Enhanced and Switchable Silicon-Vacancy Photoluminescence in Air-Annealed Nanocrystalline Diamond Films. *Carbon N. Y.* **2020**, *156*, 242–252. https://doi.org/10.1016/j.carbon.2019.09.054.

(56) Yu, B.; Yang, B.; Li, H.; Lu, J.; Huang, N.; Liu, L.; Jiang, X. Effect of Surface Oxidation on Photoluminescence of Silicon Vacancy Color Centers in the Nanocrystalline Diamond Films. *Appl. Surf. Sci.* **2021**, *552*, 149475. https://doi.org/10.1016/j.apsusc.2021.149475.

(57) Eremchev, I. Y.; Neliubov, A. Y.; Boldyrev, K. N.; Ralchenko, V. G.; Sedov, V. S.; Kador, L.; Naumov, A. V. Microscopic Insight into the Inhomogeneous Broadening of

Zero-Phonon Lines of GeV – Color Centers in Chemical Vapor Deposition Diamond Films Synthesized from Gaseous Germane. *J. Phys. Chem. C* **2021**, *125* (32), 17774–17785. https://doi.org/10.1021/acs.jpcc.1c02617.

(58) Arend, C.; Appel, P.; Becker, J. N.; Schmidt, M.; Fischer, M.; Gsell, S.; Schreck, M.; Becher, C.; Maletinsky, P.; Neu, E. Site Selective Growth of Heteroepitaxial Diamond Nanoislands Containing Single SiV Centers. *Appl. Phys. Lett.* **2016**, *108* (6), 063111. https://doi.org/10.1063/1.4941804.

(59) Görlitz, J.; Herrmann, D.; Thiering, G.; Fuchs, P.; Gandil, M.; Iwasaki, T.; Taniguchi, T.; Kieschnick, M.; Meijer, J.; Hatano, M.; Gali, A.; Becher, C. Spectroscopic Investigations of Negatively Charged Tin-Vacancy Centres in Diamond. *New J. Phys.* **2020**, *22* (1), 013048. https://doi.org/10.1088/1367-2630/ab6631.

(60) Janssen, W.; Turner, S.; Sakr, G.; Jomard, F.; Barjon, J.; Degutis, G.; Lu, Y.-G.; D'Haen, J.; Hardy, A.; Bael, M. Van; Verbeeck, J.; Tendeloo, G. Van; Haenen, K. Substitutional Phosphorus Incorporation in Nanocrystalline CVD Diamond Thin Films. *Phys. status solidi - Rapid Res. Lett.* **2014**, *8* (8), 705–709. https://doi.org/10.1002/pssr.201409235.

(61) Philip, J.; Hess, P.; Feygelson, T.; Butler, J. E.; Chattopadhyay, S.; Chen, K. H.; Chen, L. C. Elastic, Mechanical, and Thermal Properties of Nanocrystalline Diamond Films. *J. Appl. Phys.* **2003**, *93* (4), 2164–2171. https://doi.org/10.1063/1.1537465.

(62) Meesala, S.; Sohn, Y.-I.; Pingault, B.; Shao, L.; Atikian, H. A.; Holzgrafe, J.; Gündoğan, M.; Stavrakas, C.; Sipahigil, A.; Chia, C.; Evans, R.; Burek, M. J.; Zhang, M.; Wu, L.; Pacheco, J. L.; Abraham, J.; Bielejec, E.; Lukin, M. D.; Atatüre, M.; Lončar, M. Strain Engineering of the Silicon-Vacancy Center in Diamond. *Phys. Rev. B* **2018**, *97* (20), 205444. https://doi.org/10.1103/PhysRevB.97.205444.

(63) Maity, S.; Shao, L.; Sohn, Y.-I.; Meesala, S.; Machielse, B.; Bielejec, E.; Markham,

M.; Lončar, M. Spectral Alignment of Single-Photon Emitters in Diamond Using Strain Gradient. *Phys. Rev. Appl.* **2018**, *10* (2), 024050. https://doi.org/10.1103/PhysRevApplied.10.024050.

(64) Habka, N.; Barjon, J.; Lazea, A.; Haenen, K. Stress in (110)-Textured Phosphorus-Doped Polycrystalline Diamond Studied by Raman and Cathodoluminescence Spectroscopies. *J. Appl. Phys.* **2010**, *107* (10), 103531. https://doi.org/10.1063/1.3428452.

(65) Boldyrev, K. N.; Sedov, V. S.; Vanpoucke, D. E. P.; Ralchenko, V. G.; Mavrin, B. N. Localized Vibrational Modes of GeV-Centers in Diamond: Photoluminescence and First-Principles Phonon Study. *Diam. Relat. Mater.* **2022**, 109049. https://doi.org/10.1016/j.diamond.2022.109049.

(66) Siampour, H.; Wang, O.; Zenin, V. A.; Boroviks, S.; Siyushev, P.; Yang, Y.; Davydov, V. A.; Kulikova, L. F.; Agafonov, V. N.; Kubanek, A.; Mortensen, N. A.; Jelezko, F.; Bozhevolnyi, S. I. Ultrabright Single-Photon Emission from Germanium-Vacancy Zero-Phonon Lines: Deterministic Emitter-Waveguide Interfacing at Plasmonic Hot Spots. *Nanophotonics* **2020**, *9* (4), 953–962. https://doi.org/10.1515/nanoph-2020-0036.

(67) Jahnke, K. D.; Sipahigil, A.; Binder, J. M.; Doherty, M. W.; Metsch, M.; Rogers, L. J.; Manson, N. B.; Lukin, M. D.; Jelezko, F. Electron-Phonon Processes of the Silicon-Vacancy Centre in Diamond. *New J. Phys.* **2015**, *17* (4), 043011. https://doi.org/10.1088/1367-2630/17/4/043011.

(68) Razgulov, A. A.; Lyapin, S. G.; Novikov, A. P.; Ekimov, E. A. Low-Temperature Photoluminescence Study of SnV Centers in HPHT Diamond. *Diam. Relat. Mater.* **2021**, *116*, 108379. https://doi.org/10.1016/j.diamond.2021.108379.

(69) Razgulov, A. A.; Lyapin, S. G.; Novikov, A. P.; Ekimov, E. A. Low-Temperature

Photoluminescence Study of GeV Centres in HPHT Diamond. *J. Lumin.* **2022**, *242* (August 2021), 118556. https://doi.org/10.1016/j.jlumin.2021.118556.

(70) Grudinkin, S. A.; Feoktistov, N. A.; Bogdanov, K. V; Baranov, M. A.; Golubev, V. G.; Baranov, A. V. Effect of Reactive Ion Etching on the Luminescence of GeV Color Centers in CVD Diamond Nanocrystals. *Nanomaterials* **2021**, *11* (11), 2814. https://doi.org/10.3390/nano11112814.